Medical Physics
The International Journal of Medical Physics Research and Practice

A new method to retrieve phase information for equiangular fan beam differential phase contrast computed tomography

Zhao Wu, Kun Gao, Zhili Wang, Xin Ge, Jian Chen, Dajiang Wang, Zhiyun Pan, Kai Zhang, Peiping Zhu, and Ziyu Wu

Citation: Medical Physics **40**, 031911 (2013); doi: 10.1118/1.4791672
View online: http://dx.doi.org/10.1118/1.4791672
View Table of Contents: http://scitation.aip.org/content/aapm/journal/medphys/40/3?ver=pdfcov
Published by the American Association of Physicists in Medicine

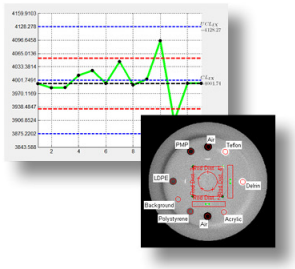

A new method to retrieve phase information for equiangular fan beam differential phase contrast computed tomography

Zhao Wu, Kun Gao, Zhili Wang,[a] Xin Ge, Jian Chen, Dajiang Wang, and Zhiyun Pan
National Synchrotron Radiation Laboratory, University of Science and Technology of China, Hefei 230029, China

Kai Zhang
Institute of High-Energy Physics, Chinese Academy of Sciences, Beijing 100049, China

Peiping Zhu and Ziyu Wu[b]
National Synchrotron Radiation Laboratory, University of Science and Technology of China, Hefei 230029, China and Institute of High-Energy Physics, Chinese Academy of Sciences, Beijing 100049, China

(Received 4 May 2012; revised 25 January 2013; accepted for publication 29 January 2013; published 25 February 2013)

Purpose: Sample radiation damage is one of the main drawbacks limiting applications of the x-ray phase-contrast imaging method. Recently, for x-ray grating-based phase contrast imaging, the reverse projection (RP) method has been proposed by Zhu *et al.* [Proc. Natl. Acad. Sci. U.S.A. **107**, 13576–13581 (2010)]. Compared to the conventional phase stepping technique, the RP method allows a strong reduction of the exposure time and minimization of the errors induced by mechanical vibrations. However, so far, it has only been considered for parallel beam illumination, typical of a synchrotron radiation source. In this paper, a generalization of the RP method from parallel beam geometry to fan beam geometry was presented and discussed.
Methods: Within parallel beam geometry, the RP method utilizes the conjugate characteristic between reverse projection images. Nevertheless, this characteristic is not directly satisfied for fan beam geometry. In this study, a phantom composed of known materials was constructed and the projection images of the phantom were calculated in a fan beam geometry. By considering single ray, the conjugate images of the projection images were derived from the projection dataset. After that, using the modified RP method the authors retrieved phase and absorption information from paired images.
Results: Extracted phase and absorption information of the phantom were in good agreement with theoretical values. Additionally, the slice reconstruction was performed and the results turned out to be in the authors' expectation.
Conclusions: Theoretical calculations and numerical simulations confirm both feasibility and validity of the RP method under fan beam illumination. Because this method is simple, fast, and releases a relatively low dose, the authors believe that this research is very useful for the x-ray phase contrast imaging applications in clinical diagnosis, bioresearch, and industrial nondestructive testing.
 [http://dx.doi.org/10.1118/1.4791672]

Key words: x-ray imaging, differential phase contrast, conjugate projection images, fan beam geometry, computed tomography

I. INTRODUCTION

Over the past decades, x-ray differential phase contrast imaging (DPCI) based on grating interferometry has been widely studied and important results have been achieved.[1–10] Thanks to its high contrast to soft tissues and the combination with computed tomography (CT),[11] the x-ray differential phase contrast computed tomography (DPC-CT) is a powerful method to observe internal structures of weekly absorbing materials. It may be then extremely helpful in many applications,[4,5,9] particularly in clinical diagnosis, biological researches, and industrial nondestructive testing. However, the large radiation dose[12,13] associated to the conventional phase stepping (PS) method[14] is one of the main drawbacks and hinders its applications in many imaging researches and in real devices. The PS method, as the standard approach, is widely used to extract phase information. However, at least three images at each tomographic viewing angle have to be collected. Recently, Zhu *et al.* presented an original relatively low dose, simple, and fast phase extraction method: the reverse-projection (RP) method[1] working with parallel beam geometry. The method collects only one image at each tomographic viewing angle by extending the scanning range from 180° to 360°, and accomplishes a dose reduction of at least 33%. Compared to the PS method, an improvement of the image quality can be also obtained via minimization of mechanical errors. However, the RP method was mainly introduced to run experiments using synchrotron radiation source and working with parallel beam layouts.[1,15] In practical applications, various nonparallel beam geometries are used in medical imaging, biology researches, and industrial nondestructive testing. It is, therefore, important to exploit the performances of different beam geometries and identify possible approaches compatible with nonparallel beam geometries.

Fan beam geometry is one of the typical nonparallel beam geometries, classified into two categories: equiangular imaging with cylindrical imaging components and equidistant imaging using planar imaging components. Due to the high aspect ratio required by a grating dedicated to high energy x-ray, planar gratings severely limit the field of view (FOV) of fan beam imaging system.[16,17] Actually, this problem can be ruled out in equiangular imaging, thanks to the inherent compatibility between fan beam geometry and cylindrical elements.

The purpose of this paper is to discuss how the RP method may retrieve phase information from projection images within equiangular fan beam geometry. A Shepp-Logan phantom made of known materials has been considered and the imaging procedure of the phantom with grating interferometer was simulated. Results show an excellent agreement and the method inherits the property of both fast and low dose working with parallel beam geometry. Foreseeable applications of this method using available x-ray differential phase contrast imaging may trigger important advancements in the field.

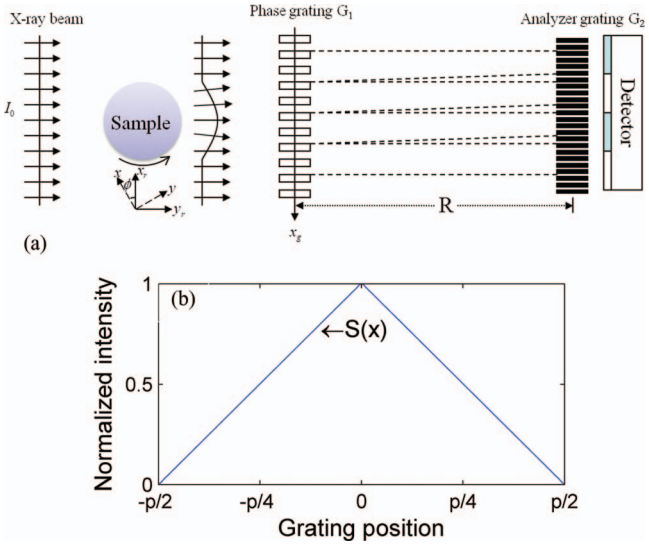

FIG. 1. Layout of the grating interferometer (a) and its shifting curve (b). p in panel (b) is the pitch of the analyzer grating G_2, see the text for more details.

II. METHODS

II.A. The RP method and its modified form for fan beam geometry

Because of the sharp reduction of the acquisition time and of the dose, the RP method is a real advancement in x-ray phase contrast imaging. Actually, the RP method takes advantage of the antisymmetry (the same absorption but the opposite differential phase via a 180° rotation) in CT projection images. Indeed, both phase and absorption information can be extracted by a proper combination of reverse projection images instead of collecting three or more projection images at each tomographic viewing angle as required by the PS method. However, the case is different and the original method is not applicable in fan beam geometry. In order to overcome this limitation, we present here a modified approach.

First, let us recall simply the RP method in parallel beam geometry. The typical setup of a grating interferometer and the shifting curve are shown in Fig. 1. Using the notations in the figure, the intensity recorded by the detector just behind the grating interferometer can be written as

$$I(x_r, \phi, z) = I_0 \exp\left[-\int_{-\infty}^{\infty} \mu(x, y, z)\, dy_r\right] S\left(\frac{x_g}{R} + \theta_r\right), \tag{1}$$

where ϕ is the rotation angle between the x_r axis and the x axis around the z axis (i.e., the rotation angle of the sample or the tomographic viewing angle) as shown in Fig. 1(a). I_0 is the intensity of the incident beam, μ denotes the linear attenuation coefficient of the sample, the function S is the shifting curve, x_g is the relative displacement between the two gratings along the x_r direction, R means the fractional Talbot distance, and $\theta_r = -\int_{-\infty}^{\infty} \partial\delta(x, y, z)/\partial x_r dy_r$ is the refraction angle with δ being the decrement of the real part of the refractive index. Here, we introduce two sets of coordinates: (x, y, z) is a rotational reference frame fixed on the sample, while (x_r, y_r, z) is a stationary reference frame with y_r along the optical axis.

In the ideal case the shifting curve is a triangular function described in Fig. 1(b), while it becomes a cosine-like curve in a real experiment for the flaws of grating, partial coherence effects of source, noise blurring, and other contributions. When the refraction angle is small, the shifting curve can be replaced by the first-order Taylor expansion at its half slope. Within the linear approximation and the antisymmetric feature, we can deduce the equations as follows:

$$\int_{-\infty}^{\infty} \mu(x, y, z)\, dy_r = \ln\left(\frac{2S\left(x_g/R\right) I_0}{I(x_r, \phi, z) + I(-x_r, \phi + \pi, z)}\right)$$

$$\int_{-\infty}^{\infty} \frac{\partial\delta(x, y, z)}{\partial x_r} dy_r = -\frac{1}{C}\frac{I(x_r, \phi, z) - I(-x_r, \phi + \pi, z)}{I(x_r, \phi, z) + I(-x_r, \phi + \pi, z)}, \tag{2}$$

where $C = \frac{1}{S(x_g/R)} \frac{dS(x_g/R)}{d\theta}$ is a constant.

From the discussions above, we may demonstrate that in parallel beam geometry the principle of the RP method is based on the antisymmetric characteristic. The critical issue is now to adapt it to fan beam geometry. Figures 2(a) and 2(b) show a schematic diagram of the reverse projection for

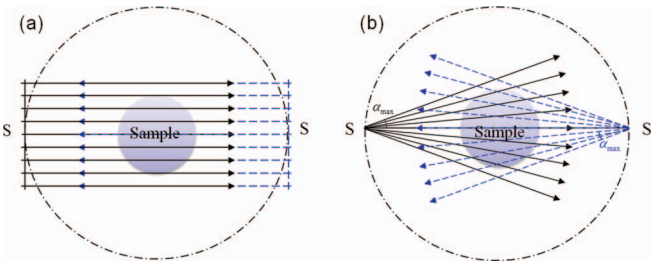

FIG. 2. The reverse projection for parallel beam (a) and fan beam (b) geometry.

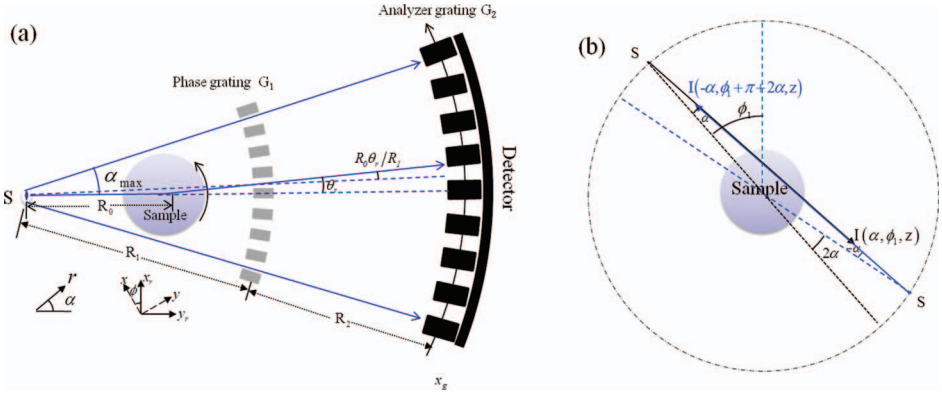

FIG. 3. Layout of the fan beam grating-based interferometer (a) and calculation of the reverse ray (b). In panel (a) G_1 and G_2 are cylindrical phase grating and absorption grating, respectively. The cylindrical detector is just behind G_2.

parallel beam and fan beam geometry, respectively. We can see that, within fan beam geometry, both absorption and differential phase do not fulfill the antisymmetry condition between reverse projection images. Consequently, the above formulas have to be modified for fan beam geometry.

In fan beam CT reconstruction, projection data are complete when the scanning range is larger than $\pi + 2\alpha_{\max}$, where $\alpha_{\max}$ is the maximum fan angle shown in Fig. 3(a). Actually, the scanning mode of the RP method is a complete circular scan. In this way, projection data are sufficient for an exact reconstruction. Taking advantage of the RP method, phase information can be extracted according to the following procedure (that we refer next as the "indirect method"): At first we rearrange the projection data of fan beam geometry to that of parallel beam geometry; then we retrieve phase and absorption information from rearranged data using the original RP method. Although this procedure is feasible, errors introduced cannot be neglected because of a large number of interpolations. Then, to minimize interpolation errors we introduce a novel method that considers a unitary ray $I(\alpha_1, \phi_1, z)$ and its reverse ray $I(\alpha_2, \phi_2, z)$. From the geometrical relationship exhibited in Fig. 3(b), we have

$$\phi_2 = \phi_1 + \pi + 2\alpha_1, \alpha_2 = -\alpha_1, \tag{3}$$

where α and ϕ are, respectively, the fan and the tomographic viewing angles, and the subscript is used to distinguish two rays. Within this new framework an antisymmetric configuration between mutual reverse rays occurs. Considering single ray, the conjugate images of projection images can be calculated. It is possible to demonstrate that the amount of interpolation errors in this process is almost half of that of the indirect method. Furthermore, when some reverse rays are directly present in the projection dataset, interpolation errors further decrease.

Based on the setup and the scale factor[18,19] of fan beam geometry shown in Fig. 3(a), the intensity recorded by the detector can be expressed as

$$I(\alpha, \phi, z) = I_0 \exp\left[-\int_{-\infty}^{\infty} \mu(x, y, z)\, dr\right] S\left(\frac{x_g}{R_2} + \frac{R_0}{R_1}\theta_r\right), \tag{4}$$

where (α, r, z) are the coordinates of the fixed cylindrical reference frame related to the x-ray beam with its origin at the position of the source. R_0, R_1, and R_2 are the distances, respectively, from the source to the center of the sample, between the source and the phase grating G_1, and from G_1 to the analyzer grating G_2, and x_g denotes the displacement of G_2 along the circular arc. Other parameters are the same as Eq. (1). From geometrical considerations we may show that the coordinate systems (α, r, z) and (x, y, z) satisfy the following relationships:

$$\begin{aligned}
\begin{pmatrix} x \\ y \\ z \end{pmatrix} &= \begin{pmatrix} \cos\phi & -\sin\phi & 0 \\ \sin\phi & \cos\phi & 0 \\ 0 & 0 & 1 \end{pmatrix} \begin{pmatrix} x_r \\ y_r \\ z \end{pmatrix} \\
&= \begin{pmatrix} \cos\phi & -\sin\phi & 0 \\ \sin\phi & \cos\phi & 0 \\ 0 & 0 & 1 \end{pmatrix} \begin{pmatrix} r\sin\alpha \\ r\cos\alpha - R_o \\ z \end{pmatrix} \\
&= \begin{pmatrix} r\sin(\alpha - \phi) + R_o \sin\phi \\ r\cos(\alpha - \phi) - R_o \cos\phi \\ z \end{pmatrix}.
\end{aligned} \tag{5}$$

Under fan beam illumination, when the refraction angle satisfies the condition $\theta_r < \frac{R_1}{R_0}\frac{d_2}{4R_2}$, with d_2 being the period of G_2, the shifting curve can be linearly approximated near its half slope. Consequently, the formulae for information retrieval can be expressed as follows:

$$\begin{aligned}
&\int_{-\infty}^{\infty} \mu(x, y, z)\, dr \\
&= \ln\left(\frac{2S(\alpha_g) I_0}{I(\alpha, \phi, z) + I(-\alpha, \phi+\pi+2\alpha, z)}\right) \\
&= A(\alpha, \phi, z) \\
&\quad - \int_{-\infty}^{\infty} \frac{\partial \delta(x, y, z)}{r\,\partial\alpha} dr \\
&= \frac{R_1}{C R_0} \frac{I(\alpha, \phi, z) - I(-\alpha, \phi+\pi+2\alpha, z)}{I(\alpha, \phi, z) + I(-\alpha, \phi+\pi+2\alpha, z)} \\
&= \theta_r(\alpha, \phi, z),
\end{aligned} \tag{6}$$

where $C = \frac{1}{S(x_g/R_2)} \frac{dS(x_g/R_2)}{d\theta}$ is a constant.

According to the equiangular fan beam reconstruction formulas,[20–24] the linear absorption coefficient and the decrement of the real part of the refractive index can be obtained by

$$\mu(x, y, z) = \int_0^{2\pi} \frac{1}{L^2} [A(\alpha, \phi, z) R_0 \cos\alpha] * \frac{\alpha^2}{\sin^2(\alpha)} H(\alpha)|_{\alpha=\alpha_0} d\phi,$$

$$\delta(x, y, z) = -\int_0^{2\pi} \frac{1}{L} [\theta_r(\alpha, \phi, z) R_0 \cos\alpha] * \frac{1}{\sin(\alpha)} I(\alpha)|_{\alpha=\alpha_0} d\phi,$$

$$L = \sqrt{R_0^2 + x^2 + y^2 + 2R_0(x\sin\phi - y\cos\phi)},$$

$$H(\alpha) = \int_{-\infty}^{\infty} |\rho| e^{j2\pi\alpha\rho} d\rho,$$

$$I(\alpha) = \int_{-\infty}^{\infty} \frac{|\rho|}{2\pi j\rho} e^{j2\pi\alpha\rho} d\rho,$$

$$\alpha_0 = \arcsin\frac{x\cos\phi + y\sin\phi}{L}, \quad (7)$$

where $H(\alpha)$ and $I(\alpha)$ are the corresponding filter functions.

In addition to fan beam geometry, cone beam geometry is another widely used illumination pattern. However, it is hard dealing with cone beam illumination using the same approach because of the incomplete projection dataset of a regular circular scan for slice reconstruction. However, work is in progress to extend the RP approach also to cone beam geometry.

II.B. Simulations

MATLAB simulations were performed to validate the proposed algorithm. To obtain the simulated projection images, the imaging process depicted in Fig. 3(a) has been performed with 25 keV x-rays. A modified Shepp-Logan phantom of 5.12×5.12 cm^2 was chosen as the sample [see Fig. 4(a)]. Its inner structure is an ellipse with a major axis of 4.68 cm and a minor axis of 3.52 cm. Each component of the phantom was filled with known materials, whose parameters, including scientific name, chemical formula, and the refractive index are listed in Table I. Data can be also found at the url http://henke.lbl.gov/optical_constants/getdb2.html.

The center of the sample was set at the optical axis, 40 cm away from the source. The $\pi/2$ phase grating G_1 with a pitch of 4 μm was situated 8.38 cm after the center of the sample. The analyzer grating G_2 with a pitch of 6 μm was located at the first fractional Talbot distance[25] $R_2 = 24.19$ cm downstream G_1. The cylindrical detector was set just behind G_2.

For numerical simulations, the sample is immersed in water, so the difference of the refractive index relative to water is extracted and reconstructed. We considered the x-ray source

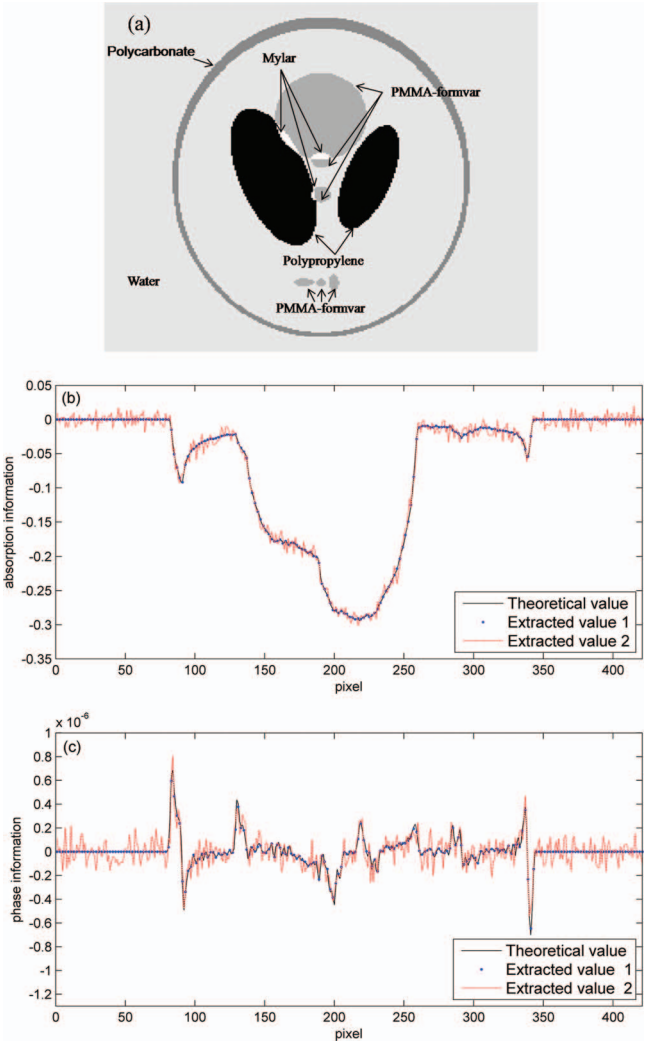

FIG. 4. Comparison among theoretical value, extracted information without noise (extracted value 1) and extracted information with noise (extracted value 2): (a) layout of the sample composition. (b) and (c) are projections of the planar sample at the tomographic viewing angle of 66° for $\Delta\mu$ and $\Delta\delta$, respectively.

intensity distribution as a Gaussian function with a standard deviation σ_s and $2\sqrt{\ln 4}\sigma_s$ represents the source size. Therefore, the coherence function of the nth harmonic is expressed as[26]

$$\eta_n = e^{(-(\pi n d_1 \sigma_s/\lambda R_1)^2/2)} \quad n = 0, \pm 1, \pm 2, \ldots,$$

where d_1 denotes the period of G_1, λ is the wavelength. σ_s was set to be 2 μm, i.e., the source size was about 5 μm and n was chosen from -101 to 101 in the simulation. Each image has been recorded with 1 s exposure. The simulation procedure performed with MATLAB comprised the following six steps:

1. Calculate the map of the refraction angle (i.e., the differential phase) and the absorption according to the integral definitions (hereafter, named as theoretical value) at any tomographic viewing angle (here we choose 66°). The detector sampling interval is $\pi/7200$.

TABLE I. Parameters of materials filled in the phantom. δ, β are, respectively, the decrement of the real part and the imaginary part of the refractive index and $\Delta\delta$, $\Delta\beta$ are the values relative to water.

Materials	Chemical formula	δ (10^{-7})	$\Delta\delta$ (10^{-7})	β (10^{-10})	$\Delta\beta$ (10^{-10})
Water	H_20	3.68889403	0	1.71446260	0
PMMA-formvar	$C_5H_8O_2$	4.26474287	0.57584884	1.53049601	−0.18396659
Polycarbonate	$C_{16}H_{14}O_3$	4.20156255	0.51266852	1.41665860	−0.29780400
Polypropylene	C_3H_6	3.41018279	−0.27871124	0.969277367	−0.745185233
Mylar	$C_{10}H_8O_4$	4.84072586	1.15183183	1.79315965	0.07869705

2. Calculate the projection image with and without the Poisson noise according to the formula of the intensity (see Refs. 24 and 25 for more details) of the grating interferometer.
3. Repeat the steps above for 360 viewing angles uniformly distributed in 360°.
4. Calculate the conjugate images of the projection images with the proposed method.
5. Extract both differential phase and absorption information from projection images with (i.e., extracted value 2) and without (i.e., extracted value 1) noise according to Eq. (6).
6. Reconstruct a slice by the filtered back-projection (FBP) method given by Eq. (7).

III. RESULTS AND DISCUSSIONS

Figure 4 shows theoretical and extracted projection information of the difference of the refraction angle and of the linear attenuation coefficient $\Delta\mu = 4\pi\Delta\beta/\lambda$ relative to water at the tomographic viewing angle of 66°, with $\Delta\beta$ being the difference of the imaginary part of the refractive index. The angle of 66° is a random choice and it is typical. We can see that extracted phase and absorption value from the projection images without noise are in good agreement with theoretical values. The noise effects are obvious, especially on the extracted refraction angle. Actually, a high frequency filter can be used to reduce them. In our simulation, the average number of photons recorded at each detector pixel is about 6000, and noise contribution can be further suppressed by increasing the exposure time and/or the photon flux. Typically, a Talbot-Lau interferometer may be employed to increase the photon flux.

We also performed a slice reconstruction from the sinogram of the extracted data without noise shown in Figs. 5(c) and 5(d), using the conventional FBP method. The reconstruction results are shown in Figs. 5(e) and 5(f). A comparison confirms the agreement between reconstructed results and the sample. For a quantitative evaluation, the correlation coefficient[27] provides a classical criterion of similarity between two images. Calculated values for the refraction angle and the linear attenuation coefficient are, respectively, 0.99994 and 0.99985, which supports the accuracy of the proposed extraction method.

In Fig. 6, we present profiles at the position indicated by dotted lines in Figs. 5(c)–5(f). We can see that the profiles of the sinogram of the extracted values almost coincide with theoretical values in Figs. 6(a) and 6(b). Moreover, profiles of the reconstruction results in Figs. 6(c) and 6(d) demonstrate that the extraction approach can be usefully applied to CT imaging.

In the derivation in Sec. II.A, a unitary ray was considered as an ideal line rather than a sector. Actually, the detector has a definite pixel size, and as a consequence the paths of a ray and its reverse ray do not overlap completely. Assuming that the critical ratio of magnifications at the exit position and at the entrance position of x-ray is 1.2, we calculated a maximum fan beam angle of 10.4318°. This is sufficient for most fan beam imaging. In this simulation, the maximum fan angle is 10.3859° larger than the critical angle of 5° that distinguishes fan beam geometry from parallel beam geometry.[22] Therefore, the illumination is a typical fan beam configuration rather than an approximate parallel beam configuration. Additional simulations were also performed to test this claiming (please see two reference simulations in Sec. IV). This is a very important issue that supports the proposed extension of the RP method to fan beam illumination.

We have discussed the condition that the sample is located at a position between the source and G_1 ($0 < R_0 < R_1$). For the case of $R_1 < R_0 < R_1 + R_2$, as shown in Fig. 7, we obtain

$$I(\alpha, \phi, z) = I_0 \exp\left[-\int_{-\infty}^{\infty} \mu(x, y, z)\, dr\right] \times S\left(\frac{x_g}{R_2} + \frac{R_1 + R_2 - R_0}{R_2}\theta_r\right) \quad (8)$$

and we may easily deal this condition in the same way. According to Eq. (2) the extraction formulae then

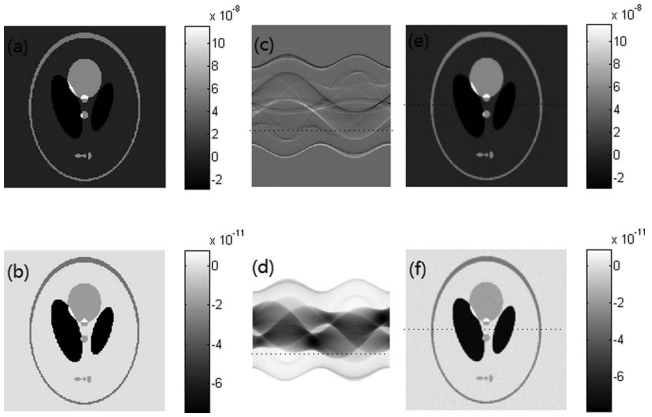

FIG. 5. Comparison of the slice reconstruction results of the difference of the refractive index relative to water: (a) and (b) are, respectively, $\Delta\delta$ and $\Delta\beta$. Panels (c), and (d) show the sinogram of the extracted information without noise, while panels (c) and (f) are the corresponding reconstructed results.

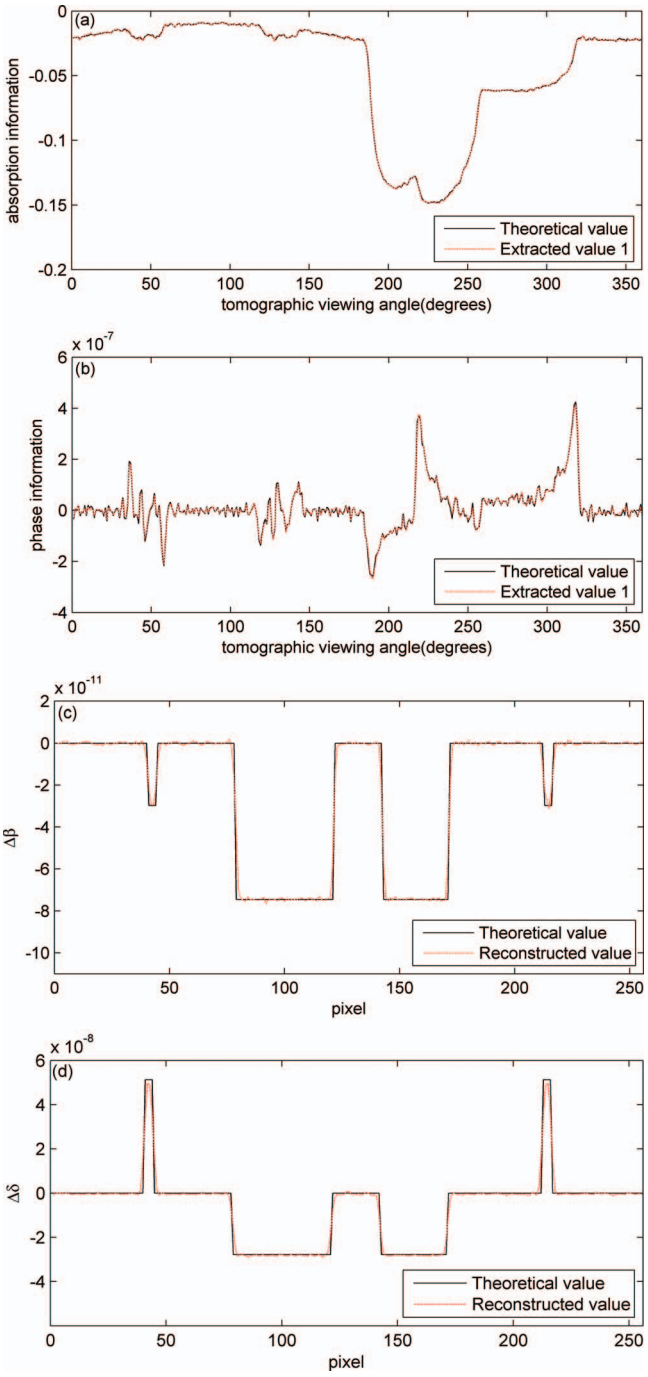

FIG. 6. Comparison of the profiles corresponding to the positions indicated in Fig. 5 by the dotted lines.

become

$$\int_{-\infty}^{\infty}\mu(x,y,z)\,dr = \ln\left(\frac{2S(\alpha_g)I_0}{I(\alpha,\phi,z)+I(-\alpha,\phi+\pi+2\alpha,z)}\right) = A(\alpha,\phi,z)$$

$$\int_{-\infty}^{\infty}\frac{\partial\delta(x,y,z)}{r\partial\alpha}dr = -\frac{R_2}{C(R_1+R_2-R_0)} \times\frac{I(\alpha,\phi,z)-I(-\alpha,\phi+\pi+2\alpha,z)}{I(\alpha,\phi,z)+I(-\alpha,\phi+\pi+2\alpha,z)} = \theta_r(\alpha,\phi,z), \quad (9)$$

where $C = \frac{1}{S(x_g/R_2)}\frac{dS(x_g/R_2)}{d\theta}$ is a constant.

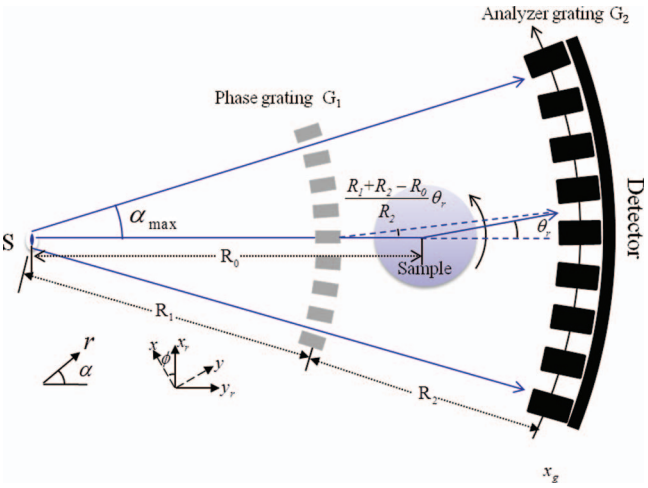

FIG. 7. Layout of imaging system with the sample located behind G1.

In the imaging system we considered, cylindrical gratings are critical optical elements that represent a challenging task for the present manufacturing technology. However, recently two teams have reported the successful fabrication of cylindrical gratings. Revol *et al.* manufactured cylindrical gratings with radii of curvature larger than 50 mm by forcing the gratings onto a cylindrical metal frame.[17] Thuering *et al.* used titanium substrates for the fabrication of cylindrically bent gratings and achieved a bending radius below 50 mm.[16] Actually, the modified RP method can be also employed with planar gratings at a relative low energy. We can easily realize this goal by transforming the length argument to the

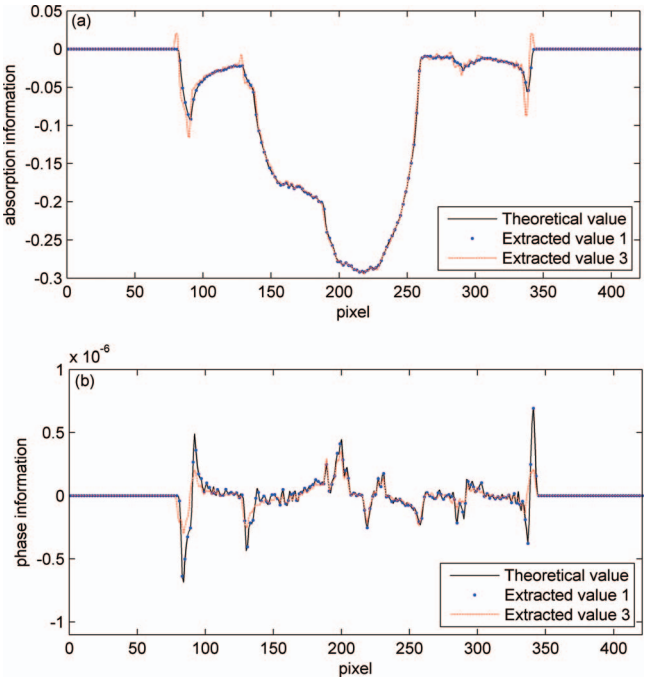

FIG. 8. Comparison among the theoretical value, the information extracted, respectively, by the modified (extracted value 1) and original (extracted value 3) RP method: (a) and (b) are projections of the planar sample at the tomographic viewing angle of 66° for $\Delta\mu$ and $\Delta\delta$, respectively.

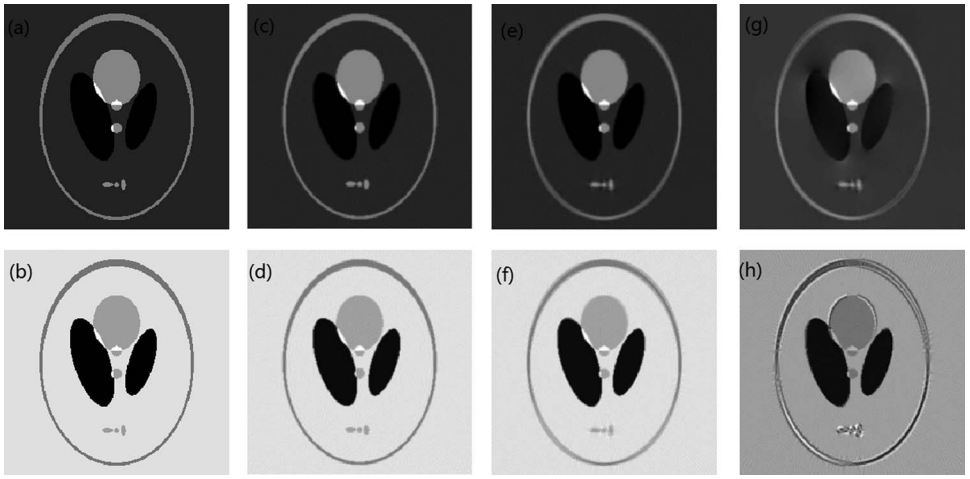

FIG. 9. Comparison of the slice reconstruction results of the difference of the refractive index relative to water: (a) and (b) are, respectively, original values of $\Delta\delta$ and $\Delta\beta$. Panels (c) and (d) show the results obtained by our method. Panels (e)–(h) show the reconstructed results of the first and the second reference simulation, respectively.

corresponding angle[28] and by reconstructing data with the equidistant reconstruction algorithm. Considering the maximum fan beam angle 10.4318°, the aspect ratio of a planar grating is limited to 22 for purpose of the largest FOV. Nevertheless, working at higher energies, gratings with high aspect ratio are required and the FOV of an imaging system based on planar gratings is significantly reduced.

IV. CONCLUSIONS

In this paper, the RP method has been analytically generalized to fan beam geometry. Although many interpolations in the calculation of the conjugate projection images have to be performed, good results are achieved. When some reverse rays are directly present in the projection dataset, fewer interpolation errors occur in the calculation of conjugate images. We also took into account the effects of the quantum noise. Nevertheless, because the detector pixel has a finite size, a unitary ray cannot be considered as an ideal line and its physical dimensions limit the maximum fan beam angle. Finally, the simulation was performed using a monochromatic x-ray illumination, while beam hardening effects[29] due to a polychromatic x-ray illumination should be considered in a real experimental layout.

In summary, thanks to the advantage of the phase-contrast CT for detecting internal structure in soft tissues and the reduction of the acquisition time and radiation dose, the RP method represents a new important tool for 3D imaging of soft tissues. Further improvements of the method may trigger DPC-CT applications in clinical medicine and biology achieving important advances in the relevant domains.

In order to support the necessity of the proposed method, two specific simulations have been performed. In the first case, we extracted information with the modified RP method but reconstructed data using the parallel beam reconstruction algorithm. In the second case, we extracted information with the parallel beam RP method and reconstructed data with the parallel beam reconstruction algorithm. The information extracted by the parallel beam RP method is mentioned as extracted value 3 exhibited in Fig. 8.

As expected, being far from the center, the extracted value 3 shows a poor agreement. The results demonstrate that the fan beam angle is too large to be handled with the parallel beam RP method. Figure 9 exhibits the reconstructed results. The main structures of the sample are in fan beam angle of 6.7074°, almost close to the critical angle of 5°. This explains why few artifacts and blurring appear in Figs. 9(e) and 9(f). However, there are so obvious errors in Figs. 9(g) and 9(h) that the results cannot reflect the real value of the sample. Comparison of these results points out that the critical fan beam angle distinguishing fan beam geometry from parallel beam geometry in the extraction method is smaller than that in the reconstruction algorithm.

ACKNOWLEDGMENTS

The authors would like to thank Augusto Marcelli (LNF-INFN) for many constructive suggestions. This work was partly supported by the National Basic Research Program of China (2012CB825800 and 2009CB930804), the Knowledge Innovation Program of the Chinese Academy of Sciences (KJCX2-YW-N42), the National Natural Science Foundation of China (NSFC 11179004, 10979055, 11205189, and 11205157), the Fundamental Research Funds for the Central Universities (WK2310000021), and the China Postdoctoral Science Foundation (2011M501064).

[a]Electronic mail: wangnsrl@ustc.edu.cn
[b]Electronic mail: wuzy@ustc.edu.cn

[1]P. P. Zhu, K. Zhang, Z. L. Wang, Y. J. Liu, X. S. Liu, Z. Y. Wu, S. A. McDonald, F. Marone, and M. Stampanoni, "Low-dose, simple, and fast grating-based x-ray phase-contrast imaging," Proc. Natl. Acad. Sci. U.S.A. **107**, 13576–13581 (2010).
[2]F. Pfeiffer, T. Weitkamp, O. Bunk, and C. David, "Phase retrieval and differential phase-contrast imaging with low-brilliance x-ray sources," Nat. Phys. **2**, 258–261 (2006).

[3]F. Pfeiffer, M. Bech, O. Bunk, P. Kraft, E. F. Eikenberry, C. Brönnimann, C. Grünzweig, and C. David, "Hard-x-ray dark-field imaging using a grating interferometer," Nat. Mater. **7**, 134–137 (2008).
[4]G. H. Chen, J. Zambelli, N. Bevins, Z. H. Qi, and K. Li, "X-ray phase sensitive imaging methods: Basic physical principles and potential medical applications," Curr. Med. Imaging Rev. **6**, 1–10 (2010).
[5]S. A. Zhou and A. Brahme, "Development of phase-contrast x-ray imaging techniques and potential medical applications," Phys. Med. **24**, 129–148 (2008).
[6]A. Momose, "Recent advances in x-ray phase imaging," Jpn. J. Appl. Phys. **44**, 6355–6367 (2005).
[7]A. Momose, W. Yashiro, and Y. Takeda, "Sensitivity of x-ray phase imaging based on Talbot interferometry," Jpn. J. Appl. Phys. **47**, 8077–8080 (2008).
[8]A. Tapfer, M. Bech, B. Pauwels, X. Liu, P. Bruyndonckx, A. Sasov, J. Kenntner, J. Mohr, M. Walter, J. Schulz, and F. Pfeiffer, "Development of a prototype gantry system for preclinical x-ray phase-contrast computed tomography," Med. Phys. **38**, 5910–5914 (2011).
[9]M. Bech, T. H. Jensen, R. Feidenhans, O. Bunk, C. David, and F. Pfeiffer, "Soft-tissue phase-contrast tomography with an x-ray tube source," Phys. Med. Biol. **54**, 2747–2753 (2009).
[10]N. Bevins, J. Zambelli, K. Li, Z. H. Qi, and G. H. Chen, "Multicontrast x-ray computed tomography imaging using Talbot-Lau interferometry without phase stepping," Med. Phys. **39**, 424–428 (2012).
[11]A. C. Kak and M. Slaney, *Principles of Computerized Tomography Imaging*, 1st ed. (IEEE, New York, 1988).
[12]D. J. Brenner and E. J. Hall, "Computed tomography - An increasing source of radiation exposure," N. Engl. J. Med. **357**, 2277–2284 (2007).
[13]J. Zambelli, N. Bevins, Z. H. Qi, and G. H. Chen, "Radiation dose efficiency comparison between differential phase contrast CT and conventional absorption CT," Med. Phys. **37**, 2473–2479 (2010).
[14]T. Weitkamp, A. Diaz, C. David, F. Pfeiffer, M. Stampanoni, P. Cloetens, and E. Ziegler, "X-ray phase imaging with a grating interferometer," Opt. Express **13**, 6296–6304 (2005).
[15]Z. L. Wang, K. Gao, J. Chen, X. Ge, P. P. Zhu, Y. C. Tian, and Z. Y. Wu, "A new method for information retrieval in two-dimensional grating-based x-ray phase contrast imaging," Chin. Phys. B **21**, 118703-1–118703-7 (2012).
[16]T. Thuering, P. Modregger, T. Grund, J. Kenntner, C. David, and M. Stampanoni, "High resolution, large field of view x-ray differential phase contrast imaging on a compact setup," Appl. Phys. Lett. **99**, 041111–041114 (2011).
[17]V. Revol, C. Kottler, R. Kaufmann, I. Jerjen, T. Luthi, F. Cardot, P. Niedermann, U. Straumann, U. Sennhauser, and C. Urban, "X-ray interferometer with bent gratings: Towards larger fields of view," Nucl. Instrum. Methods Phys. Res. A **648**, S302–S305 (2011).
[18]M. Engelhardt, J. Baumann, M. Schuster, C. Kottler, F. Pfeiffer, O. Bunk, and C. David, "High-resolution differential phase contrast imaging using a magnifying projection geometry with a microfocus x-ray source," Appl. Phys. Lett. **90**, 224101–224104 (2007).
[19]T. Donath, M. Chabior, F. Pfeiffer, O. Bunk, E. Reznikova, J. Mohr, E. Hempel, S. Popescu, M. Hoheisel, M. Schuster, J. Baumann, and C. David, "Inverse geometry for grating-based x-ray phase-contrast imaging," J. Appl. Phys. **106**, 054703–154710 (2009).
[20]Z. H. Qi and G. H. Chen, "Direct fan-beam reconstruction algorithm via filtered back-projection for differential phase-contrast computed tomography," X-Ray Opt. Instrum. **2008**, 1–8 (2008).
[21]Z. H. Qi and G. H. Chen, "A local region of interest image reconstruction via filtered backprojection for fan-beam differential phase-contrast computed tomography," Phys. Med. Biol. **52**, N417–N423 (2007).
[22]G. H. Chen and Z. H. Qi, "Image reconstruction for fan-beam differential phase contrast computed tomography," Phys. Med. Biol. **53**, 1015–1025 (2008).
[23]Z. F. Huang, K. J. Kang, Z. Li, P. P. Zhu, Q. X. Yuan, W. X. Huang, J. Y. Wang, D. Zhang, and A. M. Yu, "Direct computed tomographic reconstruction for directional-derivative projections of computed tomography of diffraction enhanced imaging," Appl. Phys. Lett. **89**, 041124–041127 (2006).
[24]F. Pfeiffer, C. Kottler, O. Bunk, and C. David, "Hard x-ray phase tomography with low-brilliance sources," Phys. Rev. Lett. **98**, 108105–108109 (2007).
[25]A. Momose, S. Kawamoto, I. Koyama, Y. Hamaishi, K. Takai, and Y. Suzuki, "Demonstration of x-ray talbot interferometry," Jpn. J. Appl. Phys. **42**, L866–L868 (2003).
[26]W. Yashiro, Y. Takeda, and A. Momose, "Efficiency of capturing a phase image using cone-beam x-ray Talbot interferometry," J. Opt. Soc. Am. **25**, 2025–2039 (2008).
[27]J. L. Starck, F. Murtagh, and A. Bijaoui, *Image Processing and Data Analysis* (Cambridge University Press, Cambridge, 1998).
[28]Z. Wu, Z. L. Wang, K. Gao, K. Zhang, X. Ge, D. J. Wang, S. H. Wang, J. Chen, Z. Y. Pan, P. P. Zhu, and Z. Y. Wu, "A generalized reverse projection method for fan beam geometry under partially coherent illumination," Radiat. Phys. Chem. (in press).
[29]M. Chabior, T. Donath, C. David, O. Bunk, M. Schuster, C. Schroer, and F. Pfeiffer, "Beam hardening effects in grating-based x-ray phase-contrast imaging," Med. Phys. **38**, 1189–1195 (2011).